Analyst

PAPER

View Article Online
View Journal | View Issue

Cite this: *Analyst*, 2016, **141**, 3090

High performance optical oxygen sensors based on iridium complexes exhibiting interchromophore energy shuttling†

Santiago Medina-Rodríguez,[a] Sergey A. Denisov,[b] Yanouk Cudré,[c] Louise Male,[c] Marta Marín-Suárez,[a] Alberto Fernández-Gutiérrez,[a] Jorge F. Fernández-Sánchez,*[a] Arnaud Tron,[b] Gediminas Jonusauskas,[d] Nathan D. McClenaghan*[b] and Etienne Baranoff*[c]

Received 29th February 2016,
Accepted 14th April 2016

DOI: 10.1039/c6an00497k

www.rsc.org/analyst

A doubly pyrene-grafted bis-cyclometallated iridium complex with engineered electronically excited states demonstrates reversible electronic energy transfer between adjacent chromophores giving rise to extremely long-lived red luminescence in solution (τ = 480 μs). Time-resolved spectroscopic studies afforded determination of pertinent photophysical parameters including rates of energy transfer and energy distribution between constituent chromophores in the equilibrated excited molecule (*ca*. 98% on the organic chromophores). Incorporation into a nanostructured metal–oxide matrix (AP200/19) gave highly sensitive O_2 sensing films, as the detection sensitivity was 200–300% higher than with the commonly used PtTFPP and approaches the sensitivity of the best O_2-sensing dyes reported to date.

Introduction

From food packaging to electronics and from beer fermentation to blood analysis, monitoring concentrations of molecular oxygen is crucial in life and environmental sciences.[1–9] The use of optical sensors for determining oxygen concentration has gained particular interest in recent years[10–19] due to their advantageous characteristics: they are simple, fast, sensitive, accurate, non-invasive, non-destructive, and they are much simpler in terms of instrumental implementation and sample preparation than traditional electrochemical methods.[7] Additionally, optical sensors can be prepared in several formats (planar, nanoparticles, paints, fibre-optic, *etc*.) and sizes, and they allow remote monitoring as well as wireless readout.[7,20]

The oxygen-sensitive luminescent dye is a central component to the optical sensor. As the excited dye has to be quenched by the triplet ground state of molecular oxygen, phosphorescent complexes based on heavy metals such as Ir(III), Pt(II), Pd(II), Re(I) and Ru(II) complexes have been particularly studied, which correspond to kinetic and energetic prerequisites.[6,7,10,21–31] The lifetime of the emissive excited state, τ_0, and hence likelihood to interact with diffusing O_2, is a key parameter influencing the performance of the sensor, which is evaluated by measuring the Stern–Volmer constant $K_{SV} = k_q \cdot \tau_0$ with k_q being the quenching rate constant. Consequently, the most commonly used highly sensitive dyes to date are Pd(II)/Pt(II) porphyrins such as Pt/PdTFPP (TFPP = *meso*-tetra(pentafluorophenyl)porphin) that have excited triplet state lifetime >50 μs, possibly reaching milliseconds for Pd porphyrins.[21,22,32] Increasing the lifetime of the excited triplet state of dyes is therefore an appealing strategy to improve the performance of the oxygen sensor.[33–37] To this end, the triplet state of organic and metalloid-containing organic molecules has been successfully harnessed for highly sensitive O_2-sensing systems due to lifetime of excited states easily reaching values >milliseconds. For example, C_{70} (τ_0 > 20 ms) reached $K_{SV} \approx 230\ kPa^{-1}$ using ethyl cellulose as the matrix.[34] Aluminum complexes of 6-hydroxy-*7H*-benzo[*de*]anthracen-7-one (τ_0 = 350 ms) reach $K_{SV} \approx 330\ kPa^{-1}$ when highly O_2-permeable Teflon AF is used as the supporting matrix.[36] However, in these cases, k_q is low ($k_q(C_{70}) \approx 11.5\ Pa^{-1}\ s^{-1}$ and k_q(Al complex) $\approx 0.94\ Pa^{-1}\ s^{-1}$) compared to iridium

[a]*Department of Analytical Chemistry, Faculty of Sciences, University of Granada, Avenida Fuentenueva s/n, 18071 Granada, Spain. E-mail: jffernan@ugr.es*
[b]*Université Bordeaux/CNRS, ISM, 351 cours de la Libération, 33405 Talence Cedex, France. E-mail: nathan.mcclenaghan@u-bordeaux.fr*
[c]*School of Chemistry, University of Birmingham, Edgbaston B15 2TT, UK. E-mail: e.baranoff@bham.ac.uk*
[d]*Université Bordeaux/CNRS, LOMA, 351 cours de la Libération, 33405 Talence Cedex, France*

† Electronic supplementary information (ESI) available: Synthetic details, crystallographic data, cyclic voltammograms, experimental details for spectroscopic and O_2 sensing studies. CCDC 1452045 and 1452046. See DOI: 10.1039/c6an00497k

complexes. For example, N969 (K_{SV1}(0–10% O_2) = 4.79 kPa^{-1} and τ_0 = 3.8 μs)[32] and EB146 (K_{SV1}(0–10% O_2) = 1.70 kPa^{-1} and τ_0 = 1.9 μs)[32] have k_q values around 1000 Pa^{-1} s^{-1}. Such compounds are therefore very promising as highly sensitive O_2-sensing dyes for ultra-low O_2 concentrations upon greatly extending the lifetime of the excited state (*i.e.* >100 μs).

Much effort has been devoted to increasing the excited state lifetime of emissive transition metal complexes. The strategies used rely upon modification of the ligands to modify the energetics of the ^{3}MLCT and ^{3}MC states[38–41] or to modify the geometry around the metal centre.[42] Another strategy is to design systems containing additional weakly interacting chromophores resulting in reversible electronic energy transfer (REET) between the core complex and the appended organic chromophore(s).[43–47] The latter strategy is very effective at significantly increasing the excited state lifetime without changing other parameters such as energetics (emission wavelength, redox potentials) and photoluminescence quantum yields and has been successfully applied to cyclometallated iridium complexes.[47–49] Surprisingly, REET has not been widely adopted for oxygen sensing beyond gaining insights into the photophysical processes occurring in the systems[50,51] or simply measuring the emission intensity ratio between air-equilibrated and degassed solutions. We have found only one report of a bichromophoric ruthenium-pyrene system exhibiting REET actually used for O_2-sensing related application, a pressure sensitive paint.[52] Yet this system has very low sensitivity to oxygen, 0.11 kPa^{-1} for the main component, which is unsuitable for measuring low concentrations of oxygen.

In this work we demonstrate with a series of dyes, Ir0, Ir1 and Ir2, that REET can be used to improve the sensitivity of low concentration oxygen sensing dyes far beyond commonly used platinum(II) porphyrins and approaches the best sensitivities reported to date. The dyes are based on a bis-cyclometallated iridium core complex of the type $Ir(C^N)_2(bpy)^+$ with C^N = 2-(naphthalen-1-yl)pyridine and bpy = 2,2′-bipyridine substituted with 0, 1 and 2 pyrene moieties (Scheme 1). It was anticipated that the two auxiliary pyrene groups would substantially increase the luminescence lifetime of Ir2 compared to that of complex Ir1 with a single appended pyrene (due to entropy-induced modification of the effective driving force for energy transfer, which favours location of excitation energy on organic chromophores in the former case exalting the energy reservoir effect), and hence greatly benefit the oxygen sensing performance, without compromising the emission profile and quantum yield of emission.[44]

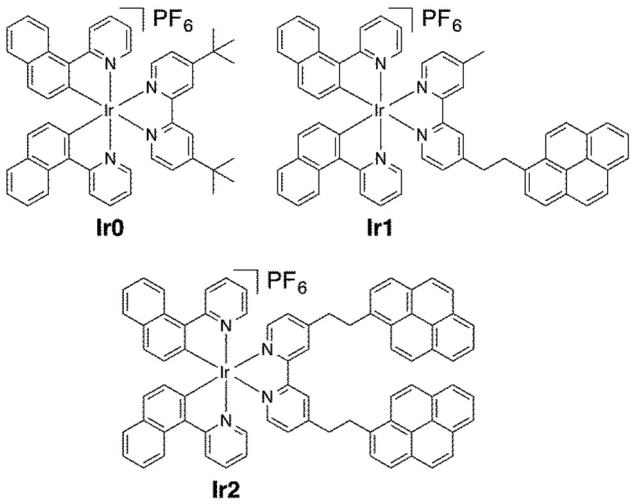

Scheme 1 Series of iridium complexes studied in this work.

Results and discussion

Synthesis and characterisation

The syntheses of Ir0 and Ir1 have been reported previously.[48] Notably, while Ir0 was obtained following standard procedures reacting the naphthylpyridine-based chloro-bridged dinuclear iridium complex directly with ^{t}Bubpy (^{t}Bubpy = 4,4′-di-tert-butyl-2,2′-bipyridine), Ir1 necessitated a synthetic strategy involving an intermediate bis-solvato iridium complex to be obtained pure. Ir2 was therefore synthesized directly with the latter strategy and obtained as an orange solid with a yield of 58%. The complex was characterized by ^{1}H NMR, high-resolution mass spectrometry (HRMS), and its purity assessed by elemental analysis. Slow diffusion of hexane into CH_2Cl_2 solutions of Ir1 and Ir2 afforded single crystals suitable for X-ray diffraction analysis. The ORTEP diagrams of both iridium complexes and crystallographic parameters are given in ESI.†

Electrochemistry

Redox potentials were measured for the three complexes in acetonitrile (Table 1). Ir0 shows only quasi-reversible oxidation of the iridium ion and reduction of the bipyridine ancillary ligand as expected for such bis-heteroleptic iridium complexes. Upon addition of a pyrene group in Ir1, two irreversible signals appear at about 0.9 and −1.7 V. As the intensity of these signals increase upon addition of the second pyrene moiety in Ir2, they are attributed to the presence of the pyrene groups.[53] Nevertheless, the redox potentials of the core complex are not significantly impacted by the presence of the pyrene groups, demonstrating the absence of electronic coupling between the two chromophores, as a result of the saturated hydrocarbon spacer.

Electronic absorption spectroscopy

The photophysical properties of Ir0, Ir1 and Ir2 are summarised in Table 1. Electronic absorption spectra in acetonitrile at room temperature (Fig. 1) are dominated by ligand-centred absorption bands in the UV region and similar MLCT absorption in the visible for all studied samples. Additional pyrene absorption bands are observed in Ir1 and Ir2 compared to Ir0, which retain their vibronic fine structure implying only weak ground-state coupling between the chromophores. As such,

Table 1 Electrochemical and photophysical properties of iridium complexes Ir0, Ir1 and Ir2 in acetonitrile at room temperature

Complex	E_{ox} [a] (V)	E_{red} [a] (V)	$\lambda_{em.\ max}$ (nm)	Φ_{air} [c]	Φ_{degas} [d]	τ (μs)[e]	K_{eq}	τ_{eq} (ns)
Ir0	0.75	−1.85	590, 625	3.8×10^{-3}	10×10^{-2}	8.3 ± 0.3	—	—
Ir1	0.76 0.92[b]	−1.83 −1.76[b]	590, 625	5×10^{-4}	9.5×10^{-2}	225 ± 15	27.8 ± 2	5
Ir2	0.76 0.89[b]	−1.81 −1.73[b]	590, 625	1×10^{-4}	9.6×10^{-2}	480 ± 15	61 ± 3	1.8

[a] $E = (E_c + E_a)/2$, *vs.* $Fc^{+/0}$. [b] Only the cathodic peak is observed, E_c is given. [c] Luminescence quantum yield (Φ_{lum}) in air-equilibrated CH_3CN solution *cf.* $[Ru(bpy)_3]^{2+}$ in H_2O (bpy = 2,2′-bipyridine), $\Phi_{lum} = 0.028$.[54] . [d] Luminescence quantum yield in degassed CH_3CN solution *cf.* $[Ru(bpy)_3]^{2+}$. [e] MLCT luminescence lifetime in dilute degassed CH_3CN.

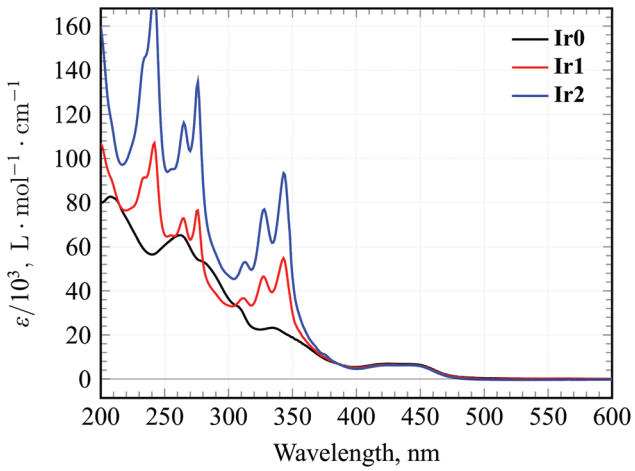

Fig. 1 Electronic absorption spectra of Ir0, Ir1 and Ir2 in acetonitrile at room temperature.

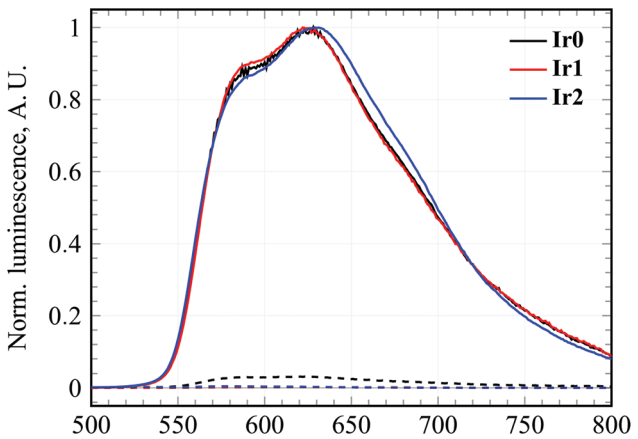

Fig. 2 Steady-state luminescence spectra of Ir0, Ir1 and Ir2 in degassed (solid) and air-equilibrated (dashed lines) acetonitrile at room temperature (λ_{exc} = 413 nm).

each chromophore is anticipated to retain its own specific properties in the ensemble.

Emission spectroscopy

Steady-state luminescence spectra show MLCT-based red emission for the complexes Ir0, Ir1 and Ir2 ($\lambda_{em.\ max}$ = 625 nm, Fig. 2), which have similar emission quantum yields in degassed acetonitrile (Φ_{degas} = 0.1). However, higher oxygen sensitivity in dilute solution is observed for Ir2 compared to Ir1 and parent Ir0. While the latter molecule shows a Φ_{degas}/Φ_{air} ratio of 26, a much higher value of 190 is obtained with Ir1 and 950 with Ir2, which is consistent with much longer excited-state lifetimes on successive introduction of pyrene chromophores. Indeed, incorporation of two pyrene chromophores is clearly advantageous in terms of prolonged emission with respect to a single pyrene. Low temperature phosphorescence measurements (77 K) showed MLCT emission ($\lambda_{em.\ max}$ = 572 nm) with Ir0, while emission emanating from dyad Ir1 and triad Ir2 was located further towards the red spectral region ($\lambda_{em.\ max}$ = 595 nm) and is ascribed to pyrene emission (see ESI†).[55,56]

A small energy gap value can be estimated at ~700 cm^{-1} between high energy emission features (see ESI†), corresponding to the energy gap between lowest lying electronically excited states on adjacent chromophores assuming similar ^{3}MLCT levels in all complexes (at room temperature similar absorption and emission spectra are observed for the emitting moiety). Note: More accurate measurements of the energy gap can be obtained through time-resolved spectroscopies, *vide infra*.

A small energy gap value is conducive with reversible inter-chromophore electronic energy transfer taking place at room temperature. This would result in an excited state equilibrium being reached, which would consequently result in prolonged luminescence lifetime and oxygen sensitivity.[44]

Time resolved spectroscopy

Time-resolved spectroscopic studies on the sub-ps to ms regimes give supplementary information on the nature of the excited molecule and a clear insight into excited-state processes in the supermolecule. An emission lifetime of 8.3 μs was obtained for Ir0 in degassed acetonitrile solution (Fig. 3), while a luminescence lifetime, which is over 25-times longer (225 ± 15 μs) was measured for a micromolar solution of Ir1, which doubled (480 ± 15 μs) for Ir2. With Ir2 proving more sensitive to O_2 and having a longer luminescence lifetime, the focus will be principally directed towards this molecule for the rest of the discussion. Additional information on Ir0 and Ir1 can be found in ref. 48.

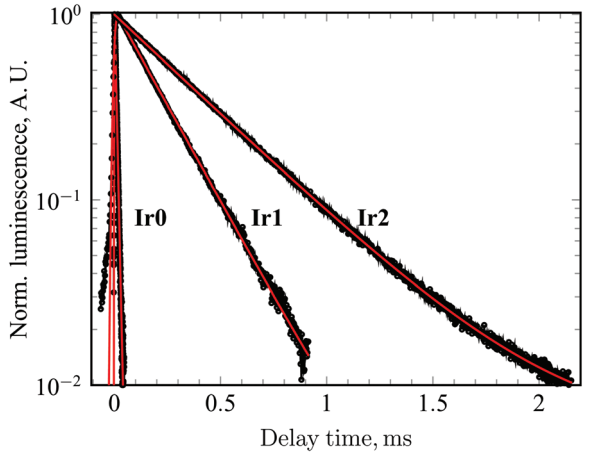

Fig. 3 Luminescence decays in the 580–620 nm range of dilute Ir0 (10 μM, λ_{exc} = 465 nm), Ir1 (2 μM, λ_{exc} = 355 nm) and Ir2 (2 μM, λ_{exc} = 355 nm) in degassed acetonitrile.

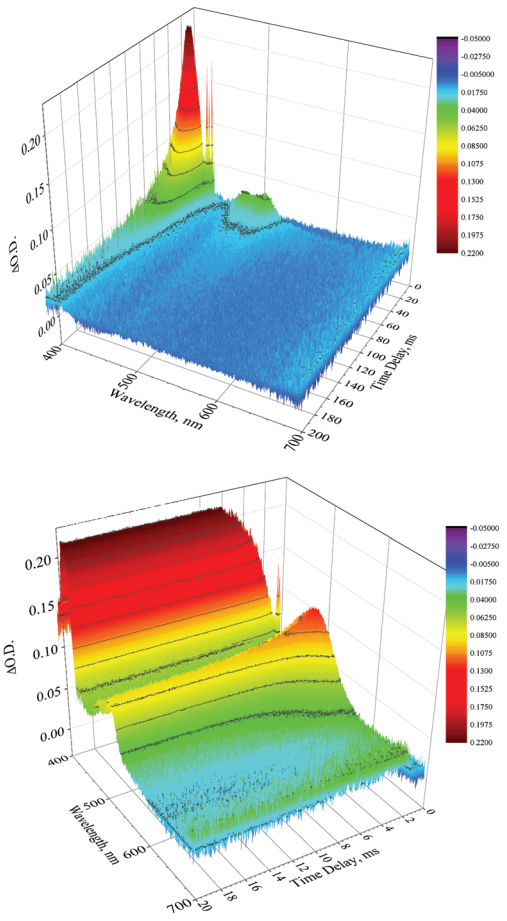

Fig. 4 Transient absorption map of Ir2 on different timescales in acetonitrile at room temperature (λ_{exc} = 430 nm, 160 μM), showing: top: real time energy distribution leading to equilibration between ^{3}MLCT and ^{3}Pyr excited states, bottom: deexcitation of the equilibrated bichromophoric molecule.

Complementary transient absorption spectroscopy studies allow elucidation of the management of energy by the excited molecule prior to emission, and transient absorption signatures for both pyrene and iridium complexes have been described.[48]

Excitation into the MLCT absorption band of Ir2 at 430 nm rapidly led to the population of the pyrene triplet, denoted by a characteristic $T_n \leftarrow T_1$ absorption at 410 nm, see Fig. 4. The kinetics of deexcitation of this absorption band exactly parallels those of the emission, clearly showing that while energy is principally located on this triplet (see ESI†), it is quantitatively transferred to the metal centre where it is subsequently emitted. This observation implies the presence of quasi-isoenergetic excited states on the adjacent chromophores permitting rapid and reversible electronic energy transfer, leading to a dynamic excited-state equilibrium.

The establishment of a dynamic excited-state equilibrium from an initial non-equilibrated excited state can be observed in real time by transient absorption spectroscopy, and a 5 ns and 1.8 ns rise time of the pyrene triplet absorption signature was measured for Ir1 and Ir2, respectively. This value gives the rate of establishment of equilibrium ($k_{eq} = 2 \times 10^8$ s^{-1} and $k_{eq} = 5.6 \times 10^8$ s^{-1}), and is equal to the sum of forward (k_f) and back (k_b) energy transfer processes.[44] The increased rate of attaining equilibrium Ir2 compared to Ir1 can be ascribed to the presence of two degenerate pyrene triplet manifolds in the former case and one in the latter complex. Due to an overlap between Ir-centre ground state bleaching signal with the transient MLCT absorption signal, the relative k_f and k_b values cannot be determined by direct observation of transient absorption signatures.

Oxygen sensing

The three Ir(III) dyes were immobilised in polystyrene (PS) and in a porous aluminium oxide solid support (AP200/19)[23,24,58] chosen for its excellent performance as supporting matrix for dyes for sensing traces of oxygen in gas.[32,59] They have been characterized by intensity measurements and the Ir(III) dye showing the best analytical performances (Ir2) was also characterised by multifrequency phase-resolved luminescence using a short duty cycle rectangular-wave as the excitation signal.[60]

The variations of the luminescence intensity with the oxygen concentration as well as the Stern–Volmer plots for Ir2-AP200/19 and Ir2-PS are shown in Fig. 5, which also demonstrate the reversibility of the sensing process. The fitting parameters for all five studied sensing films are reported in Table 2. Ir0 immobilised in AP200/19 provided very irreproducible sensing films and therefore was not studied further.

The increasing number of pyrene moieties on the complex clearly improves the oxygen sensitivity; the sensitivity of Ir2-PS is 1.5 and 5 times higher than the sensitivities of Ir1-PS and Ir0-PS, respectively, following the increase of excited state lifetime. The same effect is observed with the AP200/19 matrix, as the sensitivity of Ir2-AP200/19 is 2.4 times higher than with Ir1-AP200/19. The latter also highlights the effectiveness of the nanostructured support AP200/19 to increase the oxygen sensi-

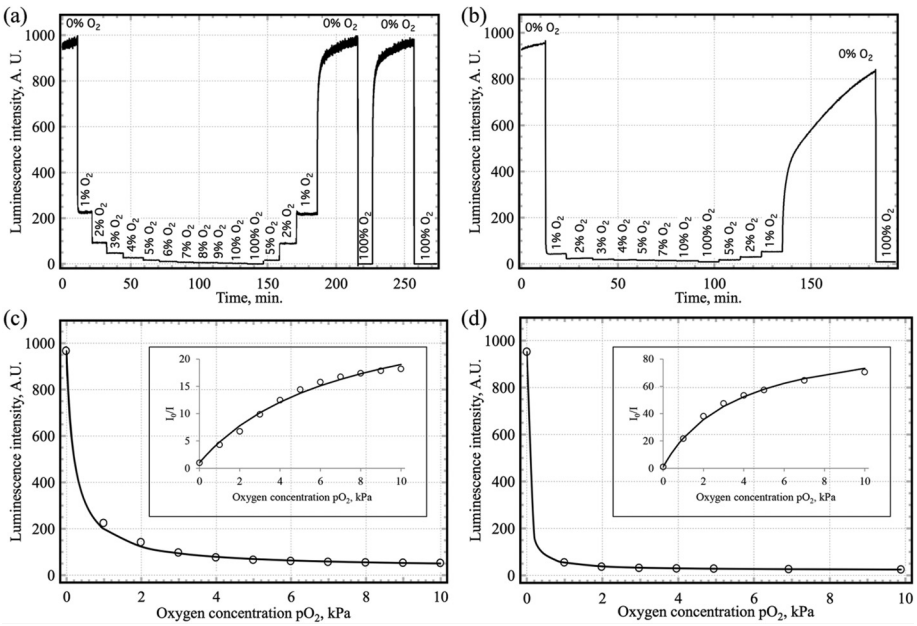

Fig. 5 Time trace curves (variation of the luminescence intensity with the oxygen concentration) for: (a) Ir2-PS and (b) Ir2-AP200/19, and calibration curves in the range 0–10 kPa O_2 and Stern–Volmer plots (I_0/I *vs.* pO_2) for (c) Ir2-PS and (d) Ir2-AP200/19 obtained by intensity measurements. Circles in (c) and (d) correspond to experimental data and lines are the mathematical fitting by using a two-site model; the parameters of the fitting have been obtained according with the ref. 57 using the criteria "a" (minimization of the square error in the analytical signal).

Table 2 Oxygen sensitivity of sensing films using luminescence intensity measurements and apparent luminescence lifetimes estimated from phase shift measurements[a]

		Intensity measurements (I_0/I)				
Range	Parameters	Ir0-PS	Ir1-PS	Ir1-AP200/19	Ir2-PS	Ir2-AP200/19
0–10 kPa pO_2	K_{SV1} (kPa^{-1})	0.87 ± 0.06[b]	2.94 ± 0.09[c]	11.03 ± 0.35[b]	4.499 ± 0.796[d]	26.96 ± 0.25[b]
	x_1	0.9 ± 0.0	1.0 ± 0.0	0.9 ± 0.1	0.9684 ± 0.006	0.99 ± 0.03
	K_{SV2} (kPa^{-1})	0.00 ± 0.00	—	0.00 ± 0.00	—	0.00 ± 0.00
	x_2	0.1 ± 0.1	—	0.1 ± 0.1	—	0.01 ± 0.01
	R^2	0.999 ± 0.007	0.9922 ± 0.0250	0.9999 ± 0.0004	0.9904 ± 0.0011	0.9998 ± 0.0009
				Apparent lifetime measurements (τ_ϕ)		
				Ir2-PS		Ir2-AP200/19
0–1 kPa pO_2	K_{SV1} (kPa^{-1})			7.99 ± 0.72[d]		94.81 ± 0.19[b]
	x_1			0.96 ± 0.01		0.76 ± 0.04
	K_{SV2}(kPa^{-1})			—		2.28 ± 0.10
	x_2			—		0.24 ± 0.03
	R^2			0.9986 ± 0.0009		0.9996 ± 0.0008
0–10 kPa pO_2	K_{SV1} (kPa^{-1})			8.79 ± 0.61[d]		45.64 ± 0.16[a]
	x_1			0.941 ± 0.002		0.90 ± 0.03
	K_{SV2} (kPa^{-1})			—		0.30 ± 0.08
	x_2			—		0.10 ± 0.02
	R^2			0.9972 ± 0.0012		0.9985 ± 0.0011

[a] [Dye concentration] = 1.5 mg mL^{-1}; the results are the average of 3 replicas $\pm st/\sqrt{n}$ (n = 3, t = 4.303 (2P = 0.05), s = standard deviation), the fitting parameters have been obtaining according with ref. 57 using criteria "a". [b] Data fitted with the Demas two-site model. [c] Data fitted with the Stern–Volmer model. [d] Data fitted with the Lehrer two-site model.

tivity, as previously observed for other oxygen sensitive dyes.[23–25,32]

Based on intensity measurements, the most sensitive sensing film is Ir2-AP200/19 (K_{SV} of 26.96 kPa^{-1}). Comparing these results with classical Pt(II), Ru(II), and Ir(III) sensing films using the same nanostructured matrix, it is clear that this sensing film is very promising for O_2-sensing applications, showing a higher Stern–Volmer constant than one of the most

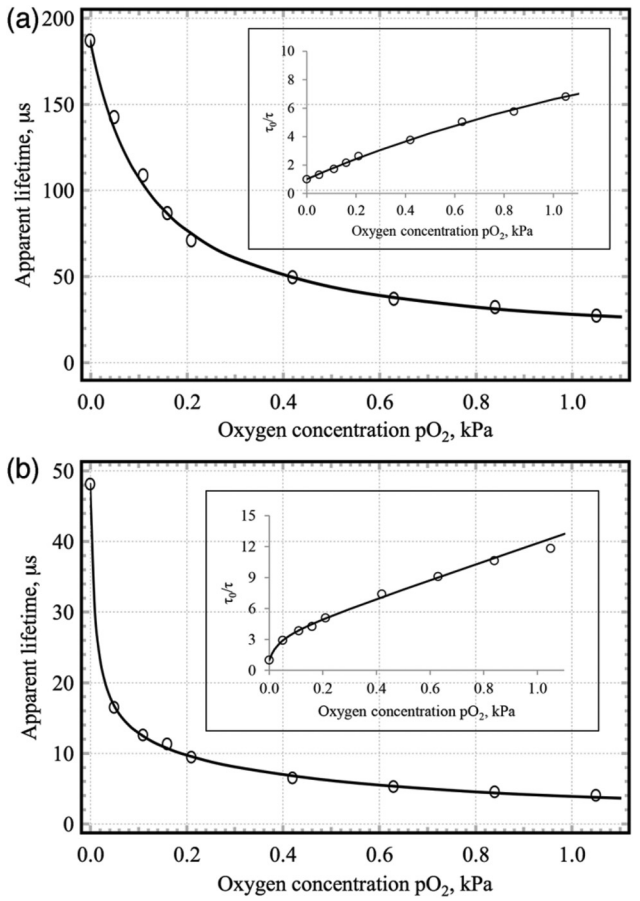

Fig. 6 Calibration curves (τ_φ, expressed in microseconds) in the range 0–1 kPa O_2 and Stern–Volmer plots (τ_0/τ *vs.* pO_2) for (a) Ir2-PS and (b) Ir2-AP200/19 at 21 °C. Circles corresponds with experimental data and lines are the mathematical fitting by using a two-site model; the parameters of the fitting have been obtained according with the ref. 57 using the criteria "a".

sensitive complexes published in the literature so far (K_{sv}(PtTFPP-AP200/19) = 25.68 kPa^{-1}).[32]

In order to determine if Ir2 can be used for analysing low oxygen concentration, lifetime measurements were carried out in the frequency domain (phase-resolved method)[32,59,60] because intensity measurements are not sensitive enough to characterize the sensing films in the ranges 0–1 and 0–0.21 kPa pO_2. The description of the methodology as well as the protocol for carrying out the measurements are described by Medina-Rodríguez *et al.*[59,60] The modulation frequencies used for the measurement in these ranges (see ESI; Fig. S11†) were 1130 Hz for the Ir2-PS sensing film (average phase difference of 51.90 degrees) and 2260 Hz for the Ir2-AP200/19 sensing film (average phase difference of 32.61 degrees). The variation of the apparent luminescence lifetime of Ir2 incorporated into PS and into AP200/19 when exposed to different oxygen concentrations between 0–1 kPa pO_2 are shown in Fig. 6 and the results are summarized in Table 2, demonstrating the high sensitivity of the film (K_{SV1} of Ir2-AP200/19 is 94.81 kPa^{-1} and $\Delta\tau_{0.05}$ of Ir2-AP200/19 = 68.51 ± 0.21%); the $\Delta\tau_{0.05}$ of PtTFPP-AP200/19 measured in the same conditions is 62.53 ± 3.66%.[32]

Finally, the measurement capability of Ir2-PS and Ir2-AP200/19 was also determined by comparing the measured oxygen concentrations with the real O_2 concentrations (see ESI, Table S2†), which shows the reliability of the sensing films.

Conclusions

In summary, the benefit of reversible intramolecular energy transfer as a strategy to improve the oxygen sensitivity of phosphorescent iridium complexes by dramatically increasing the excited state lifetime is shown herein using a series of complexes, Ir0, Ir1 and Ir2, bearing 0, 1 and 2 pyrene moieties, respectively. Ir2 presents an excited state lifetime in solution of 480 µs, almost twice the excited state lifetime of Ir1 containing only one pyrene group. Incorporation into AP200/19, a nanostructured inorganic matrix, Ir2 leads to an oxygen sensing performance (K_{SV} = 26.96 kPa^{-1}) similar to the best reported film using the same matrix, PtTFPP-AP200/19 with K_{sv} = 25.68 kPa^{-1}. This is the first time that a non-porphyrin-based transition metal complex reaches such high performance. Furthermore, using a lifetime measurement method for very low oxygen concentration 0–1 kPa, Ir2-AP200/19 provides excellent performance with Ksv = 94.81 kPa^{-1} to be compared to 31.02 kPa^{-1} for PtTFPP in the same conditions.[32] Such performance is only bested by some organic and metalloid-containing organic dyes that, however, have low k_q values (k_q < 10 Pa s^{-1}) compared to the system reported here (k_q up to ≈ 2000 Pa s^{-1}). These results clearly demonstrate the potential of reversible intramolecular energy transfer as a strategy to develop high performance oxygen sensing dyes.

A key advantage of this strategy is that it provides a rational approach to further enhancing the performance of the dyes: simply increasing the number of energy reservoir units will increase the excited state lifetime linearly, as previously demonstrated with ruthenium dyes,[61] which will result in an increase of sensitivity. Equally, reversible energy transfer could *a priori* be instilled in Pd/Pt porphyrins in an analogous fashion. Clearly ultrasensitive oxygen sensing dyes are now accessible.

Acknowledgements

The authors acknowledge Labex Laphia, ANR FOSET (ANR-12-BS08-0007-01), the Spanish Ministry of Economy and Competitiveness (CTQ2014-53442-P), the European Union (HetIridium, CIG322280), for financial support, the School of Chemistry, University of Birmingham, for a studentship, and the EPSRC for underpinning support.

Notes and references

1 S. M. Borisov, A. S. Vasylevska, C. Krause and O. S. Wolfbeis, *Adv. Funct. Mater.*, 2006, **16**, 1536.

2 J. F. Fernández-Sánchez, T. Roth, R. Cannas, M. K. Nazeeruddin, S. Spichiger, M. Graetzel and U. E. Spichiger-Keller, *Talanta*, 2007, **71**, 242.
3 C. McDonagh, C. S. Burke and B. D. MacCraith, *Chem. Rev.*, 2008, **108**, 400.
4 O. S. Wolfbeis, *Anal. Chem.*, 2008, **80**, 4269.
5 S. M. Borisov, R. Seifner and I. Klimant, *Anal. Bioanal. Chem.*, 2011, **400**, 2463.
6 K. Koren, S. M. Borisov, R. Saf and I. Klimant, *Eur. J. Inorg. Chem.*, 2011, 1531.
7 X.-d. Wang and O. S. Wolfbeis, *Chem. Soc. Rev.*, 2014, **43**, 3666.
8 R. Ramamoorthy, P. K. Dutta and S. A. Akbar, *J. Mater. Sci.*, 2003, **38**, 4271.
9 J. W. Schwank and M. DiBattista, *MRS Bull.*, 1999, **24**, 44.
10 Y. Amao, *Microchim. Acta*, 2003, **143**, 1.
11 C. A. K. Lange, P. Stavrakas, U. F. O. Luhmann, D. J. De Silva, R. R. Ali, Z. J. Gregor and J. W. B. Bainbridge, *Am. J. Ophthalmol.*, 2011, **152**, 406.
12 A. L. Medina-Castillo, J. F. Fernández-Sánchez and A. Fernández-Gutiérrez, *Adv. Funct. Mater.*, 2011, **21**, 3488.
13 K. Xie, X.-W. Zhang, L. Huang, Y.-T. Wang, Y. Lei, J. Rong, C.-W. Qian, Q.-L. Xie, Y.-F. Wang, A. Hong and S. Xiong, *Cytotechnology*, 2011, **63**, 345.
14 D. E. Achatz, R. J. Meier, L. H. Fischer and O. S. Wolfbeis, *Angew. Chem., Int. Ed.*, 2011, **50**, 260.
15 D. H. Song, H. D. Kim and K. C. Kim, *Opt. Lasers Eng.*, 2012, **50**, 74.
16 O. Ergeneman, G. Chatzipirpiridis, J. Pokki, M. Marín-Suárez, G. A. Sotiriou, S. Medina-Rodríguez, J. F. Fernández-Sánchez, A. Fernández-Gutiérrez, S. Pane and B. J. Nelson, *IEEE Trans. Biomed. Eng.*, 2012, **59**, 3104.
17 C.-S. Chu, Y.-L. Lo and T.-W. Sung, *Photonic Sens.*, 2011, **1**, 234.
18 M. Quaranta, S. M. Borisov and I. Klimant, *Bioanal. Rev.*, 2012, **4**, 115.
19 X.-d. Wang, H.-x. Chen, Y. Zhao, X. Chen, X.-r. Wang and X. Chen, *TrAC, Trends Anal. Chem.*, 2010, **29**, 319.
20 J. R. Lakowicz, *Principles of Fluorescence Spectroscopy*, Kluwer Academic, New York, 2nd edn, 1999.
21 S. M. Borisov and I. Klimant, *Anal. Chem.*, 2007, **79**, 7501.
22 S. M. Borisov, P. Lehner and I. Klimant, *Anal. Chim. Acta*, 2011, **690**, 108.
23 J. F. Fernández-Sánchez, R. Cannas, S. Spichiger, R. Steiger and U. E. Spichiger-Keller, *Anal. Chim. Acta*, 2006, **566**, 271.
24 M. Marín-Suárez del Toro, J. F. Fernández-Sánchez, E. Baranoff, M. K. Nazeeruddin, M. Gräetzel and A. Fernández-Gutiérrez, *Talanta*, 2010, **82**, 620.
25 M. Marín-Suárez, B. F. E. Curchod, I. Tavernelli, U. Rothlisberger, R. Scopelliti, I. Jung, D. Di Censo, M. Grätzel, J. F. Fernández-Sánchez, A. Fernández-Gutiérrez, M. K. Nazeeruddin and E. Baranoff, *Chem. Mater.*, 2012, **24**, 2330.
26 A. L. Medina-Castillo, J. F. Fernández-Sánchez, C. Klein, M. K. Nazeeruddin, A. Segura-Carretero, A. Fernández-Gutiérrez, M. Graetzel and U. E. Spichiger-Keller, *Analyst*, 2007, **132**, 929.
27 P. J. R. Roche, M. C. K. Cheung, K. Y. Yung, A. G. Kirk, V. P. Chodavarpu and F. V. Bright, *Sens. Actuators, B*, 2010, **147**, 581.
28 A. Mills, *Platinum Met. Rev.*, 1997, **41**, 115.
29 S. Wang, B. Li, L. Zhang, L. Liu and Y. Wang, *Appl. Organomet. Chem.*, 2011, **25**, 21.
30 Y.-J. Liu and Y.-P. Zhang, *Z. Anorg. Allg. Chem.*, 2013, **639**, 533.
31 T. Yoshihara, S. Murayama and S. Tobita, *Sensors*, 2015, **15**, 13503.
32 S. Medina-Rodríguez, M. Marín-Suárez, J. F. Fernández-Sánchez, A. de la Torre-Vega, E. Baranoff and A. Fernández-Gutiérrez, *Analyst*, 2013, **138**, 4607.
33 S. M. Borisov, R. Fischer, R. Saf and I. Klimant, *Adv. Funct. Mater.*, 2014, **24**, 6548.
34 S. Nagl, C. Baleizao, S. M. Borisov, M. Schaferling, M. N. Berberan-Santos and O. S. Wolfbeis, *Angew. Chem., Int. Ed.*, 2007, **46**, 2317.
35 G. Zhang, J. Chen, S. J. Payne, S. E. Kooi, J. N. Demas and C. L. Fraser, *J. Am. Chem. Soc.*, 2007, **129**, 8942.
36 P. Lehner, C. Staudinger, S. M. Borisov and I. Klimant, *Nat. Commun.*, 2014, **5**, 4460.
37 G. Zhang, G. M. Palmer, M. W. Dewhirst and C. L. Fraser, *Nat. Mater*, 2009, **8**, 747.
38 T. C. Harlang, Y. Liu, O. Gordivska, L. A. Fredin, C. S. Ponseca Jr., P. Huang, P. Chabera, K. S. Kjaer, H. Mateos, J. Uhlig, R. Lomoth, R. Wallenberg, S. Styring, P. Persson, V. Sundstrom and K. Warnmark, *Nat. Chem.*, 2015, **7**, 883.
39 S. Y. Takizawa, K. Shimada, Y. Sato and S. Murata, *Inorg. Chem.*, 2014, **53**, 2983.
40 S. Encinas, L. Flamigni, F. Barigelletti, E. C. Constable, C. E. Housecroft, E. R. Schofield, E. Figgemeier, D. Fenske, M. Neuburger, J. G. Vos and M. Zehnder, *Chem. – Eur. J.*, 2002, **8**, 137.
41 D. L. Ashford, C. R. Glasson, M. R. Norris, J. J. Concepcion, S. Keinan, M. K. Brennaman, J. L. Templeton and T. J. Meyer, *Inorg. Chem.*, 2014, **53**, 5637.
42 M. Abrahamsson, M. Jager, R. J. Kumar, T. Osterman, P. Persson, H. C. Becker, O. Johansson and L. Hammarstrom, *J. Am. Chem. Soc.*, 2008, **130**, 15533.
43 F. N. Castellano, *Acc. Chem. Res.*, 2015, **48**, 828.
44 A. Lavie-Cambot, C. Lincheneau, M. Cantuel, Y. Leydet and N. D. McClenaghan, *Chem. Soc. Rev.*, 2010, **39**, 506.
45 Y. Leydet, D. M. Bassani, G. Jonusauskas and N. D. McClenaghan, *J. Am. Chem. Soc.*, 2007, **129**, 8688.
46 X.-y. Wang, A. Del Guerzo and R. H. Schmehl, *J. Photochem. Photobiol., C*, 2004, **5**, 55.
47 X. Jiang, J. Peng, J. Wang, X. Guo, D. Zhao and Y. Ma, *ACS Appl. Mater. Interfaces*, 2016, **8**, 3591.
48 S. A. Denisov, Y. Cudre, P. Verwilst, G. Jonusauskas, M. Marín-Suárez, J. F. Fernández-Sánchez, E. Baranoff and N. D. McClenaghan, *Inorg. Chem.*, 2014, **53**, 2677.
49 A. J. Howarth, D. L. Davies, F. Lelj, M. O. Wolf and B. O. Patrick, *Inorg. Chem.*, 2014, **53**, 11882.

50 T. A. Grusenmeyer, J. Chen, Y. Jin, J. Nguyen, J. J. Rack and R. H. Schmehl, *J. Am. Chem. Soc.*, 2012, **134**, 7497.
51 R. Hueting, M. Tropiano and S. Faulkner, *RSC Adv.*, 2014, **4**, 44162.
52 H. F. Ji, Y. B. Shen, J. P. Hubner, B. F. Carroll, R. H. Schmehl, J. A. Simon and K. S. Schanze, *Appl. Spectrosc.*, 2000, **54**, 856.
53 S. L. Murov, I. Carmichael and G. L. Hug, *Handbook of Photochemistry*, Marcel Dekker, Inc., New York, 2nd edn, 1993.
54 H. Ishida, S. Tobita, Y. Hasegawa, R. Katoh and K. Nozaki, *Coord. Chem. Rev.*, 2010, **254**, 2449.
55 L. Peter and G. Vaubel, *Chem. Phys. Lett.*, 1973, **21**, 158.
56 M. Montalti, A. Credi, L. Prodi and M. T. Gandolfi, *Handbook of Photochemistry*, CRC Press, Boca Raton, 3rd edn, 2006.
57 S. Medina-Rodríguez, A. de la Torre-Vega, C. Medina-Rodríguez, J. F. Fernández-Sánchez and A. Fernández-Gutiérrez, *Sens. Actuators, B*, 2015, **212**, 278.
58 J. F. Fernández-Sánchez, I. Fernández, R. Steiger, R. Beer, R. Cannas and U. E. Spichiger-Keller, *Adv. Funct. Mater.*, 2007, **17**, 1188.
59 S. Medina-Rodríguez, F. J. Orriach-Fernández, C. Poole, P. Kumar, A. de la Torre-Vega, J. F. Fernández-Sánchez, E. Baranoff and A. Fernández-Gutiérrez, *Chem. Commun.*, 2015, **51**, 11401.
60 S. Medina-Rodríguez, A. de la Torre-Vega, F. J. Sainz-Gonzalo, M. Marín-Suárez, C. Elosúa, F. J. Arregui, I. R. Matias, J. F. Fernández-Sánchez and A. Fernández-Gutiérrez, *Anal. Chem.*, 2014, **86**, 5245.
61 N. D. McClenaghan, F. Barigelletti, B. Maubert and S. Campagna, *Chem. Commun.*, 2002, 602.